J|A|C|S
ARTICLES
Published on Web 12/09/2006

Dissecting and Reducing the Heterogeneity of Excited-State Energy Transport in DNA-Based Photonic Wires

Mike Heilemann,† Robert Kasper, Philip Tinnefeld,* and Markus Sauer

Contribution from Applied Laser Physics and Laser Spectroscopy, Bielefeld University, Universitätsstrasse 25, 33615 Bielefeld, Germany

Received August 2, 2006; E-mail: tinnefeld@physik.uni-bielefeld.de

Abstract: Molecular photonic wires are one-dimensional representatives of a family of nanoscale molecular devices that transport excited-state energy over considerable distances in analogy to optical waveguides in the far-field. In particular, the design and synthesis of such complex supramolecular devices is challenging concerning the desired homogeneity of energy transport. On the other hand, novel optical techniques are available that permit direct investigation of heterogeneity by studying one device at a time. In this article, we describe our efforts to synthesize and study DNA-based molecular photonic wires that carry several chromophores arranged in an energetic downhill cascade and exploit fluorescence resonance energy transfer to convey excited-state energy. The focus of this work is to understand and control the heterogeneity of such complex systems, applying single-molecule fluorescence spectroscopy (SMFS) to dissect the different sources of heterogeneity, i.e., chemical heterogeneity and inhomogeneous broadening induced by the nanoenvironment. We demonstrate that the homogeneity of excited-state energy transport in DNA-based photonic wires is dramatically improved by immobilizing photonic wires in aqueous solution without perturbation by the surface. In addition, our study shows that the in situ construction of wire molecules, i.e., the stepwise hybridization of differently labeled oligonucleotides on glass cover slides, further decreases the observed heterogeneity in overall energy-transfer efficiency. The developed strategy enables efficient energy transfer between up to five chromophores in the majority of molecules investigated along a distance of ∼14 nm. Finally, we used multiparameter SMFS to analyze the energy flow in photonic wires in more detail and to assign residual heterogeneity under optimized conditions in solution to different leakages and competing energy-transfer processes.

Introduction

One of the most important processes of molecules in the excited state is resonance energy transfer.[1] Resonance energy transfer can occur when the emission spectrum of a chromophore, called the donor, overlaps with the absorption spectrum of another molecule, called the acceptor. Nature has evolved several examples of energy-transfer systems that guide light from the light-harvesting complexes to the reaction center as initial steps of photosynthesis. Besides understanding fundamental aspects of these processes, scientists have started copying nature's principles to construct artificial light-harvesting complexes, e.g., complex multichromophoric systems and conjugated polymers, which open up interesting applications in material sciences and molecular photonics.[2−9] Exciting prospects to exploit energy-transfer processes are the development of energy-transfer relays for nanoscale sensors and the development of so-called molecular photonic wires.[10,11] In contrast to electronic wires which convey energy by the transport of electrons/holes, photonic wires support the transport of excited-state energy along a series of chromophores.

Supramolecular systems with a precise arrangement of chromophores in distance and relative orientation suited for energy transport are hard to access and can, for example, be found in some fluorescent proteins. To some degree, such systems could be synthetically realized in porphyrin arrays and rigid polymer chains end-capped by chromophores.[4,12−16] The

† Current address: Clarendon Laboratory, Department of Physics, University of Oxford, Parks Road, Oxford OX1 3PU, United Kingdom.

(1) Scholes, G. D. *Annu. Rev. Phys. Chem.* **2003**, *54*, 57−87.
(2) De Schryver, F. C.; Vosch, T.; Cotlet, M.; Van der Auweraer, M.; Muellen, K.; Hofkens, J. *Acc. Chem. Res.* **2005**, *38*, 514−522.
(3) Tinnefeld, P.; Heilemann, M.; Sauer, M. *ChemPhysChem* **2005**, *6*, 217−222.
(4) Garcia-Parajo, M. F.; Hernando, J.; Mosteiro, G. S.; Hoogenboom, J. P.; van Dijk, E. M. H. P.; van Hulst, N. F. *ChemPhysChem* **2005**, *6*, 819−827.
(5) Kim, D.; Osuka, A. *Acc. Chem. Res.* **2004**, *37*, 735−745.
(6) Barbara, P. F.; Gesquiere, A. J.; Park, S. J.; Lee, Y. J. *Acc. Chem. Res.* **2005**, *38*, 602−610.
(7) Gust, D.; Moore, T. A.; Moore, A. L. *Acc. Chem. Res.* **2001**, *34*, 40−48.
(8) Schwartz, B. J. *Annu. Rev. Phys. Chem.* **2003**, *54*, 141−172.
(9) Schindler, F.; Lupton, J. M.; Feldmann, J.; Scherf, U. *Proc. Natl. Acad. Sci. U.S.A.* **2004**, *101*, 14695−14700.
(10) Willard, D. M.; Mutschler, T.; Yu, M.; Jung, J.; Van Orden, A. *Anal. Bioanal. Chem.* **2006**, *384*, 564−571.
(11) Wagner, R. W.; Lindsey, J. S. *J. Am. Chem. Soc.* **1994**, *116*, 9759−9760.
(12) Kim, Y. H.; Jeong, D. H.; Kim, D.; Jeoung, S. C.; Cho, H. S.; Kim, S. K.; Aratani, N.; Osuka, A. *J. Am. Chem. Soc.* **2001**, *123*, 76−86.
(13) Hoeben, F. J. M.; Jonkheijm, P.; Meijer, E. W.; Schenning, A. P. H. J. *Chem. Rev.* **2005**, *105*, 1491−1546.
(14) Park, M.; Cho, S.; Yoon, Z. S.; Aratani, N.; Osuka, A.; Kim, D. *J. Am. Chem. Soc.* **2005**, *127*, 15201−15206.
(15) Hofkens, J.; Cotlet, M.; Vosch, T.; Tinnefeld, P.; Weston, K. D.; Ego, C.; Grimsdale, A.; Muellen, K.; Beljonne, D.; Bredas, J. L.; Jordens, S.; Schweitzer, G.; Sauer, M.; De Schryver, F. *Proc. Natl. Acad. Sci. U.S.A.* **2003**, *100*, 13146−13151.
(16) Cotlet, M.; Vosch, T.; Habuchi, S.; Weil, T.; Muellen, K.; Hofkens, J.; De Schryver, F. *J. Am. Chem. Soc.* **2005**, *127*, 9760−9768.

10.1021/ja065585x CCC: $33.50

degree of order in devices built-up of large molecules such as π-conjugated molecules or multichromophoric systems is of similar importance to device functionality as the chemical homogeneity and purity.[13,14,17] It is thus predicted that the control of molecular organization will become increasingly important for macroscopic electronic and optical device performance in the future. With respect to one-dimensional molecular energy-transfer systems that aim at the transport of excited-state energy, the precise arrangement of several chromophores with a high degree of order over considerable distances on the one hand and the maintenance of directionality of energy transfer on the other hand have not yet been achieved. Fluorescence resonance energy transfer (FRET) represents a sensitive mechanism to probe the relative orientations of and distances between chromophores and thus the functionality of photonic wires.

Single-molecule fluorescence spectroscopy (SMFS) is the ideal tool to explore order and heterogeneity, as ensemble averaging is avoided. Recent single-molecule studies on multichromophoric systems such as conjugated polymers and dendrimers have led to a refined understanding of their photophysics, e.g., the influence of the chain packing or the role of different energy-transfer pathways and mechanisms (see, e.g., refs 9, 15, 18−21). SMFS has also been used to unravel heterogeneity in one-dimensional photonic wires as the main source of malfunctioning and variations of energy transfer.[14,17,22,23] Park et al., for example, investigated bleaching in porphyrin arrays of different length at the single-molecule level and demonstrated a strong influence of the nanoenvironment for porphyrin arrays containing more than eight units.[14] For identical chromophores, variations in the local environment led to the formation of so-called energy sinks, disrupting the energy flow along the array.[12]

Recently, we demonstrated the successful synthesis and spectroscopic characterization of a unidirectional photonic wire based on four highly efficient energy-transfer steps between five spectrally different chromophores covalently attached to double-stranded (ds) DNA,[22] that is, the observation and investigation of the first multistep FRET between more than three chromophores at the single-molecule level. The DNA-based modular conception enabled the introduction of various chromophores at well-defined positions and arbitrary inter-chromophore distances (e.g., 10 base pairs between chromophores), which is essential to prevent dimer formation and to avoid energy sinks and leaks. While ensemble fluorescence measurements showed overall FRET efficiencies of only 15−30%, SMFS uncovered subpopulations that exhibited overall FRET efficiencies of ∼90% along a distance of 13.6 nm and a spectral range of ∼200 nm.[3,22]

DNA as a modular building block offers an elegant synthetic route to control the distances between selected chromophores, thus guaranteeing the directionality of energy transfer. On the other hand, the relative orientation of chromophores with respect to each other remains random. So far, DNA-based photonic wires carrying up to five different chromophores were studied in solution at the ensemble level and as individuals immobilized on bare glass cover slides. These previous experiments have left a considerable degree of uncertainty with respect to (i) sample preparation, i.e., chemical heterogeneity, (ii) heterogeneity induced by the nanoenvironment, (iii) complex photophysics of the chromophores, i.e., photophysical heterogeneity, and (iv) specific requirements for FRET, such as relative orientations of the transition dipoles.

In this article, we work out a strategy that addresses two main sources of heterogeneity: the physical environment and unfavorable relative orientation of the chromophores. The key of the strategy is the immobilization of photonic wires in solution with minimal perturbation by the surface. Thus, the chromophores attached to the DNA backbone can freely rotate in solution, concurrently washing out the heterogeneity of dipole orientations within the time scale of the experiment.

Since complex supramolecular systems require an individual investigation of each system, SMFS was applied. To extract maximum information and to identify common properties of subpopulations, several fluorescence parameters were monitored in parallel, i.e., emission wavelength, fluorescence lifetime, and polarization.[24−26] The distribution of the fluorescence intensity recorded on four spectrally separated channels provides a rough spectral signature acquired with high time resolution. Together with the fluorescence lifetime information, individual energy-transfer steps can be quantified. Our data demonstrate that the heterogeneity in excited-state energy transport in photonic wires composed of selected chromophores is strongly reduced by immobilization in aqueous surroundings. Furthermore, we show that surface-immobilized photonic wires prepared in situ, i.e., by stepwise hybridization of complementary oligonucleotides labeled with different chromophores to an immobilized 60mer oligonucleotide under single-molecule conditions, exhibit a high degree of homogeneity up to the incorporation of the fourth chromophore, while further elongation to the fifth chromophore was observed with lower efficiency.

Materials and Methods

Materials. All fluorescent dyes were purchased as *N*-hydroxysuccinimidyl ester (NHS-ester). ATTO590 and ATTO647N were purchased from ATTO-TEC (Siegen, Germany), Rhodamine Green (RhG) from Invitrogen (Karlsruhe, Germany), and Cy5.5 from Amersham Biosciences Europe (Freiburg, Germany). Amino-modified oligonucleotides of various lengths were purchased from IBA (Göttingen, Germany).

Synthesis of Chromophore-Labeled Oligonucleotides. Amino-modified oligonucleotides were labeled with fluorescent dyes using classical NHS-ester chemistry and standard solvents purchased from Merck (Darmstadt, Germany). To 1 equiv of oligonucleotide dissolved in 0.1 M carbonate buffer (pH 9.4) was added a 5-fold excess of NHS-ester, and this mixture was incubated for 6 h protected from light. Labeled oligonucleotides were purified by HPLC (Hewlett-Packard, Böblingen, Germany) on a reversed-phase column (Knauer, Berlin, Germany) packed with octadecylsilane−hypersil C18. Separation was

(17) Becker, K.; Lupton, J. M. *J. Am. Chem. Soc.* **2006**, *128*, 6468−6479.
(18) VandenBout, D. A.; Yip, W. T.; Hu, D. H.; Fu, D. K.; Swager, T. M.; Barbara, P. F. *Science* **1997**, *277*, 1074−1077.
(19) Yu, J.; Hu, D. H.; Barbara, P. F. *Science* **2000**, *289*, 1327−1330.
(20) Huser, T.; Yan, M.; Rothberg, L. J. *Proc. Natl. Acad. Sci. U.S.A.* **2000**, *97*, 11187−11191.
(21) Becker, K.; Lupton, J. M.; Feldmann, J.; Setayesh, S.; Grimsdale, A. C.; Muellen, K. *J. Am. Chem. Soc.* **2006**, *128*, 680−681.
(22) Heilemann, M.; Tinnefeld, P.; Sanchez Mosteiro, G.; Garcia Parajo, M.; Van Hulst, N. F.; Sauer, M. *J. Am. Chem. Soc.* **2004**, *126*, 6514−6515.
(23) Hernando, J.; de Witte Pieter, A. J.; van Dijk Erik, M. H. P.; Korterik, J.; Nolte Roeland, J. M.; Rowan Alan, E.; Garcia-Parajo Maria, F.; van Hulst Niek, F. *Angew. Chem., Int. Ed.* **2004**, *43*, 4045−4049.
(24) Ha, T.; Enderle, T.; Chemla, D. S.; Selvin, P. R.; Weiss, S. *Phys. Rev. Lett.* **1996**, *77*, 3979−3982.
(25) Tinnefeld, P.; Sauer, M. *Angew. Chem., Int. Ed.* **2005**, *44*, 2642−2671.
(26) Rothwell, P. J.; Berger, S.; Kensch, O.; Felekyan, S.; Antonik, M.; Wohrl, B. M.; Restle, T.; Goody, R. S.; Seidel, C. A. M. *Proc. Natl. Acad. Sci. U.S.A.* **2003**, *100*, 1655−1660.

performed in 0.1 M triethylammonium acetate, using a linear gradient from 0% to 75% acetonitrile over 20 min. Reaction yields were up to 85%.

Preparation of Photonic Wires. Photonic wires were synthesized by hybridization of appropriately labeled 20mer oligonucleotides to a 60mer template strand. The template strand was further modified with biotin at the 3′-end and amino-C6 at the 5′-end (5′-amino-ATC GTT ACC AAA GCA TCG TAA ATC GCA TAA TAG CAC GTT AAT TTA GCA CGG ACG ATC GCC-3′-biotin). The sequence was checked for unwanted secondary structure using *mfold*.[27] No secondary structure >2 kJ/mol was obtained, thus indicating good accessibility for hybridization. RhG served as the input unit of photonic wires and was attached to the 5′-end of the template strand. The complementary strand was split into three oligonucleotides with a length of 20 base pairs (bp) each, designed in such a way that a 10-bp distance between adjacent chromophores was realized. The first complementary strand was purchased labeled with tetramethylrhodamine (TMR), incorporated as dT-TMR at position 11, and an additional amino-C6 modification at the 5′-end. The oligonucleotide was post-labeled with ATTO590 and purified. The second single strand carried an amino-C6 linker at position 10 and was conjugated with ATTO647N. Cy5.5 was conjugated to the amino-C6-modified 5′-end of the third fragment. Hybridization of the four single-stranded oligonucleotides in phosphate-buffered saline (PBS, pH 7.4) was performed in a thermocycler, heating the sample to 90 °C and then slowly cooling to room temperature overnight. This protocol yielded DNA-based photonic wires with an active length of 14 nm, containing up to five chromophores at a distance of 10 bp.

Immobilization of Photonic Wires. Photonic wires containing a biotin tag at the 3′-end of the template strand were immobilized on streptavidin-coated surfaces as described elsewhere.[28] Measurements were performed in PBS containing 100 mM β-mercaptoethylamine (MEA) unless stated otherwise.

In an alternative synthetic route, photonic wires were built up in situ, i.e., by stepwise hybridization of oligonucleotides on the biotin-BSA/BSA surface. The RhG-labeled template strand was incubated ($\sim 10^{-8}$ M) while the density of immobilized molecules was monitored simultaneously by fluorescence scanning microscopy. At a density of $\sim$1 molecule/μm^2, the immobilization reaction was stopped by washing the surface several times with buffer. Stepwise, 10^{-8} M solutions of the complementary oligonucleotides were added, and the progress of hybridization was monitored by spectrally resolved fluorescence scanning microscopy. This procedure allowed us to construct photonic wires in a modular and flexible way from their single-stranded precursors.

Ensemble Absorption and Fluorescence Emission Spectroscopy. All measurements were carried out at room temperature (25 °C) in PBS buffer, pH 7.4. Absorption spectra were taken on a Cary 500 UV−vis−NIR spectrometer (Varian, Darmstadt, Germany). Steady-state fluorescence spectra were measured in standard quartz cuvettes with a path length of 10 or 1 mm, using a high-pressure xenon flash lamp as the excitation source. To avoid re-absorption and re-emission effects, concentrations were kept strictly below 1 μM (typically 0.1 μM).

Single-Molecule Fluorescence Experiments. Single-molecule experiments with photonic wires were performed using the confocal setup represented schematically in Figure 1A. A mode-locked Ti:sapphire laser (Tsunami, Spectra-Physics) was used for experiments with 488-nm pulsed excitation. The Ti:sapphire laser tuned to 976 nm was pumped by a 532-nm all-solid-state laser (Millennia, Spectra-Physics). The emitted light was frequency doubled using a flexible harmonic generator (GWU-Lasertechnik), generating 488-nm laser light pulses with a pulse length of 100 fs (fwhm) and a 76-MHz repetition rate. Pulse stretching with a 50-m single-mode fiber yielded ~150-ps pulses. The laser was coupled into the objective (100×, NA 1.45; Zeiss) by a dichroic beamsplitter (500DCLP, AHF Analysentechnik, Germany). Fluorescence was collected by the same objective and split onto the active areas of four APDs after spatial and spectral filtering. In front of the detectors, additional bandpass filters were used to select the desired spectral detection ranges of 503−548 (blue channel), 560−610 nm (green channel), 620−680 (yellow channel), and 680−738 nm (red channel). Figure 1B shows the transmission characteristics of the four detection channels, taking into account beamsplitters (dotted lines), filters (solid lines), and the detection sensitivity of the APDs (filled areas). Accordingly, the different detection channels have comparable detection sensitivity. The emission spectra of five representative chromophores attached to DNA oligonucleotides is shown in the same graph (from left to right: RhG, TMR, ATTO590, ATTO647N, and Cy5.5). Due to the shape of the chromophore spectra, each chromophore has a fingerprint-like intensity distribution along the four detectors. For example, the RhG fluorophore attached to DNA in aqueous solution emits 57% on the first ("blue"), 37% on the second ("green"), 5% on the third ("yellow"), and <1% on the fourth ("red") channel. Table 1 summarizes the expected intensity distributions on different channels

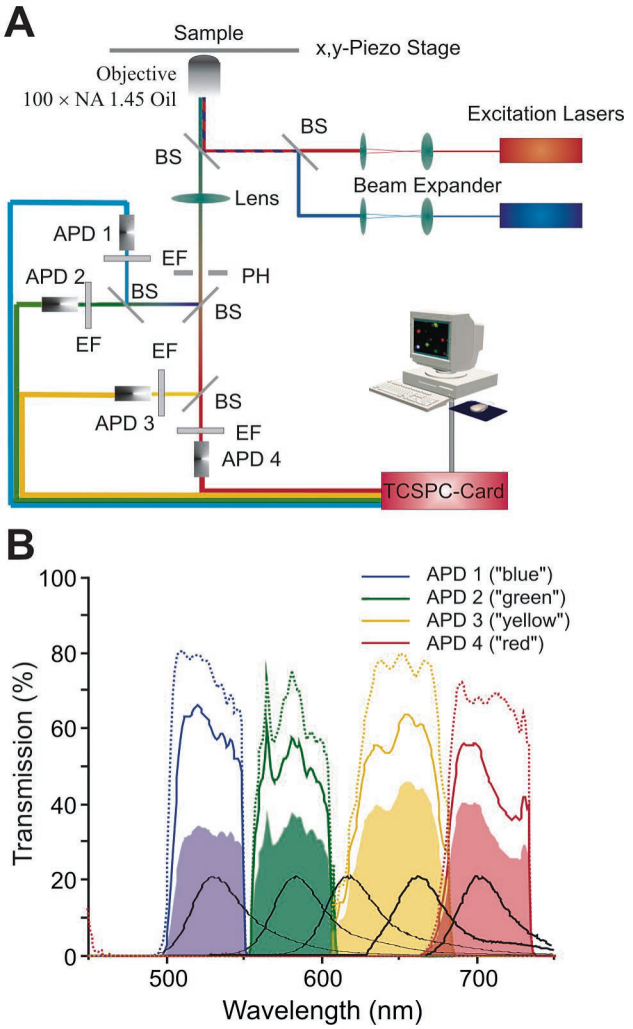

Figure 1. (A) Setup for fast spectrally resolved fluorescence lifetime measurements of single molecules on four detectors. As excitation sources, different laser sources, including the 488-nm line of an Ar^+ laser, a frequency-doubled Ti:sapphire laser operating at 488 nm, and a red laser diode (635 nm) were used. BS, beam splitter; APD, avalanche photodiode; EF, emission filter; PH, pinhole; TCSPC, time-correlated single-photon counting. (B) Transmission properties of the four detection channels, including the transmission of the dichroic beam splitters (dotted line), additionally filters (solid line), and detector sensitivity (filled areas). The emission spectra of RhG, TMR, ATTO590, ATTO647N, and Cy5.5 are additionally displayed in black from left to right.

(27) Zuker, M. *Nucleic Acids Res.* **2003**, *31*, 3406−3415.
(28) Piestert, O.; Barsch, H.; Buschmann, V.; Heinlein, T.; Knemeyer, J.-P.; Weston, K. D.; Sauer, M. *Nano Lett.* **2003**, *3*, 979−982.

Table 1. Spectroscopic Properties and Distribution of the Respective Chromophore Emissions on the Four Spectrally Separated Detection Channels[a]

fluorescent dye	λ_{abs} (nm)	λ_{em} (nm)	blue 503–547 nm	green 560–610 nm	yellow 620–680 nm	red 680–738 nm	WSM values
RhG	508	534	0.57	0.37	0.05	0.01	1.50
TMR	560	582	<0.02	0.72	0.23	0.03	2.27
ATTO590	603	625	<0.01	0.33	0.54	0.12	2.77
ATTO647N	645	661	0	<0.01	0.64	0.34	3.33
Cy5.5	683	707	0	0	<0.01	0.99	3.99

[a] See Figure 1B for comparison. The ensemble WSM values, which reflect the chromophore emission, are also given (calculation of WSM is shown in eq 2).

for the most frequently used dyes in our experiments, as determined at the ensemble level. A PC-card for time-correlated single-photon counting (TCSPC 630, Becker&Hickl, Berlin, Germany) and custom-written LabView software were used for data recording and analysis.[29] Fluorescence decays were deconvoluted and fitted using IBH Decay Analysis Software (version 6.1, Horiba Jobin Yvon). Instrument response functions were recorded with a scattering solution.

Results and Discussion

Sources of Heterogeneity in Multistep FRET Constructs. To realize DNA-based photonic wires that show highly efficient and homogeneous FRET from the first input chromophore (donor) via several transmitting chromophores to the final output chromophore (last acceptor), the parameters that contribute to heterogeneity have to be well controlled. One major source of the observed heterogeneity lies in variations in the energy-transfer efficiency E. FRET between an excited donor and an acceptor involves coupling of the molecules' transition moments via Coulombic interaction. For donor−acceptor distances within the weak coupling limit, i.e., donor−acceptor distances >2 nm, Förster derived an expression for the rate constant k_{ET} for dipole−dipole induced energy transfer (eq 1).[30]

$$k_{ET} = \frac{9000 \ln 10\, \kappa^2\, \Phi_D}{128\, \pi^5\, n^4\, N_A\, \tau_D\, R^6} \int_0^\infty \frac{F_D(\bar{\nu})\, \epsilon_A(\bar{\nu})}{\bar{\nu}^4} d\bar{\nu} \qquad (1)$$

Equation 1 expresses the rate constant for energy transfer in measurable spectroscopic quantities such as the refractive index of the medium, n, the orientation factor, κ^2, the fluorescence quantum yield of the donor, Φ_D, its fluorescence lifetime, τ_D, Avogadro's number, N_A, the normalized fluorescence spectrum of the donor, $F_D(\bar{\nu})$, the absorption spectrum of the acceptor, expressed by its extinction coefficient, $\epsilon_A(\bar{\nu})$, and the average transition frequency, $\bar{\nu}$, in cm^{-1}. Furthermore, k_{ET} depends on the donor−acceptor distance to the sixth power, R^6.[31] In DNA-based photonic wires, flexible alkyl linkers connect the chromophores to the DNA scaffold, leaving considerable conformational freedom for both R and κ^2. As it is safe to assume that the chromophores can adopt all possible orientations with respect to each other, the orientation factor κ^2 can vary from 0 to 4, and therefore its influence on energy-transfer efficiency is expected to be larger than the influence of distance variations for DNA-based photonic wires.

For studies carried out in solution, κ^2 is often assumed to be 2/3, which is the expected average value for isotropically distributed transition dipoles. The validity of this assumption depends on the local environment of the chromophores. For example, photonic wires immobilized on a bare glass surface exhibit rather fixed orientations of chromophores,[24,32] with different conformations with respect to the DNA and to each other, resulting in broadening of FRET efficiency distributions.[33,34] Therefore, it is anticipated that a broad distribution of κ^2 values contributes significantly to the large heterogeneity of energy-transfer efficiencies observed for DNA-based photonic wires immobilized on dry glass slides.[22]

Even for labeled DNA in solution, free rotation of chromophores along the DNA cannot always be assumed. The rotational mobility of chromophores attached to DNA is strongly determined by its charge, hydrophobicity, and the linker length.[35] Experimentally, the rotational mobility can be accessed through anisotropy measurements.[26,36,37] The chromophores used in this work exhibit ensemble fluorescence anisotropy values r_{aniso} in the range of 0.05−0.3 when attached to DNA, indicating intermediate rotational mobility between those of free chromophores and fixed emission dipoles. Ensemble and single-molecule spectroscopies have evidenced the existence of conformationally different chromophore−DNA interactions, exploiting selective quenching of certain chromophores by guanosine residues.[38−41] Furthermore, it was suggested that an equilibrium between these different states is achieved in the millisecond time range. Accordingly, although the relative orientation of chromophores does not completely average out to yield $\kappa^2 = 2/3$, rotation of chromophores in solution experiments should exhibit a more narrow FRET distribution as compared to that of immobilized transition dipoles. Since our approach to molecular photonic wires does not imply a chemical route to precisely arrange the transition moments with respect to each other, we suggest preserving the rotational mobility of the chromophores so that different transition dipole moment orientations average out on the time scale of the experiment.

Recently, strategies have been developed that enable immobilization of molecules while maintaining their solution

(29) Weston, K. D.; Dyck, M.; Tinnefeld, P.; Muller, C.; Herten, D. P.; Sauer, M. *Anal. Chem.* **2002**, *74*, 5342−5349.
(30) Förster, T. *Ann. Phys.* **1948**, *2*, 55−75.
(31) Clegg, R. M. *Method Enzymol.* **1992**, *211* (DNA Struct., Pt. A), 353−388.
(32) Bohmer, M.; Enderlein, J. *J. Opt. Soc. Am. B* **2003**, *20*, 554−559.
(33) Hubner, C. G.; Ksenofontov, V.; Nolde, F.; Mullen, K.; Basche, T. *J. Chem. Phys.* **2004**, *120*, 10867−10870.
(34) Talaga, D. S.; Lau, W. L.; Roder, H.; Tang, J.; Jia, Y.; DeGrado, W. F.; Hochstrasser, R. M. *Proc. Natl. Acad. Sci. U.S.A.* **2000**, *97*, 13021−13026.
(35) Norman, D. G.; Grainger, R. J.; Uhrin, D.; Lilley, D. M. J. *Biochemistry* **2000**, *39*, 6317−6324.
(36) Dietrich, A.; Buschmann, V.; Muller, C.; Sauer, M. *Rev. Mol. Biotechnol.* **2002**, *82*, 211−231.
(37) Vamosi, G.; Gohike, C.; Clegg, R. M. *Biophys. J.* **1996**, *71*, 972−994.
(38) Edman, L.; Mets, U.; Rigler, R. *Proc. Natl. Acad. Sci. U.S.A.* **1996**, *93*, 6710−6715.
(39) Eggeling, C.; Fries, J. R.; Brand, L.; Gunther, R.; Seidel, C. A. M. *Proc. Natl. Acad. Sci. U.S.A.* **1998**, *95*, 1556−1561.
(40) Sauer, M.; Drexhage, K. H.; Lieberwirth, U.; Muller, R.; Nord, S.; Zander, C. *Chem. Phys. Lett.* **1998**, *284*, 153−163.
(41) Heinlein, T.; Knemeyer, J.-P.; Piestert, O.; Sauer, M. *J. Phys. Chem. B* **2003**, *107*, 7957−7964.

environment, e.g., by binding to coated glass substrates or confining their motion inside vesicles or gels.[42−46] In this work, photonic wires were immobilized via biotinylated BSA and streptavidin/biotin chemistry using a biotinylated DNA template strand. Under these conditions, DNA fully maintains its biological and structural functionality,[28,47] which is important for our modular approach to build up photonic wires exploiting hybridization of single oligonucleotides. Immobilization of photonic wires under close to physiological conditions can also help to reduce a second source of heterogeneity, i.e., inhomogeneous broadening resulting from diverse nanoenvironments of the chromophores. This effect can be unspecific and dominated by the rigidity of the environment,[48] or specific, e.g., due to quenching pathways by photoinduced electron transfer (PET) to a neighboring donor or acceptor molecule. Partners in PET reactions can be part of the construct (e.g., nucleobases and in particular guanosine),[49,50] stem from proteins in the surrounding (here tryptophan is the key electron donor),[51,52] or be due to impurity molecules or the matrix itself.[53−58] The influence of different immobilization strategies on photophysical properties of chromophores was investigated recently.[59] While single molecules adsorbed on a dry glass surface exhibited broad distributions of emission maxima and fluorescence lifetimes, the heterogeneity could be dramatically reduced upon immobilization of the chromophores in solution.[59,60]

Photonic wires are synthesized exploiting the self-assembling properties of DNA. An essential factor controlling the homogeneity of photonic wires thus is the chemical identity of individual educts as well as the quantitative formation of the wire, consisting of four oligonucleotides carrying the corresponding chromophores. Chemical heterogeneity can be introduced by imperfect labeling of the DNA, residual unbound dyes or free DNA, incomplete hybridization, dissociation of DNA strands, and heterogeneity induced by unfavorable secondary structures of oligonucleotides. Error sources are, for example, concentration determination and are generally inherent when building up a molecule out of multiple components. For example, extinction coefficients of chromophores vary by up to 20% when the chromophores are bound to DNA, hampering concentration determination.[37] Even with the purest labeled oligonucleotides, hybridization of four oligonucleotides is generally not quantitative. Purification in native gels requires comparatively large quantities and is complicated, as the electrophoretic mobility of the DNA strands is largely controlled by the multitude of different chromophores attached. Furthermore, it is not guaranteed that a clean and chemically homogeneous sample remains homogeneous after chromatographic separation. For example, new heterogeneity can be imported upon dilution to the single-molecule level or in the course of the immobilization procedure. Therefore, a strategy was developed to build up photonic wires in situ by subsequent hybridization to the immobilized 60-bp template DNA strands, which is independent of concentration determination but features a substantial increase in hybridization yield without further purification steps.

Finally, photophysical/photochemical heterogeneity is expected in terms of premature photobleaching of chromophores, inactive chromophore populations,[61−63] and higher excited-state interactions of chromophores.[64] While proper immobilization can largely reduce heterogeneity stemming from an inhomogeneous environment, the photostability of chromophores is generally affected as well. For example, chromophores are by a factor of 10−100 less photostable when immobilized in aqueous solution compared to chromophores embedded in polymers or adsorbed on a dry glass surface.[59] For some chromophores, strategies have recently been developed to increase observation times before fluorescence is lost due to irreversible photobleaching. These strategies often involve oxygen removal, as molecular oxygen is a well-known source for photochemical processes leading to photodestruction.[65] On the other hand, oxygen removal does not improve the photostability of all chromophores. As oxygen is an efficient triplet quencher as well, opposite effects can be obtained if the prevalent photobleaching path involves higher excitations from triplet states.[66] Other popular substances used to increase photostability are reducing agents and triplet quenchers such as ascorbic acid, β-mercaptoethanol (BME), or β-mercaptoethylamine (MEA).[67]

Under the conditions of FRET, i.e., when several chromophores are confined in a small volume, additional effects leading to rapid photobleaching can occur.[64] Higher excited states of chromophores, which are often intermediates in the photobleaching path, can be populated more frequently due to annihilation processes or excitation at comparably short

(42) Dickson, R. M.; Norris, D. J.; Tzeng, Y. L.; Sakowicz, R.; Goldstein, L. S. B.; Moerner, W. E. *Mol. Cryst. Liq. Cryst. Sci. Technol. Sect. A—Mol. Cryst. Liq. Cryst.* **1996**, *291*, 31−39.
(43) Haran, G. *J. Phys.: Condens. Matter* **2003**, *15*, R1291−R1317.
(44) Groll, J.; Amirgoulova Elza, V.; Ameringer, T.; Heyes Colin, D.; Rocker, C.; Nienhaus, G. U.; Moller, M. *J. Am. Chem. Soc.* **2004**, *126*, 4234−4239.
(45) Pal, P.; Lesoine, J. F.; Lieb, M. A.; Novotny, L.; Knauf, P. A. *Biophys. J.* **2005**, *89*, L11−L13.
(46) Funatsu, T.; Harada, Y.; Tokunaga, M.; Saito, K.; Yanagida, T. *Nature* **1995**, *374*, 555−559.
(47) Okumus, B.; Wilson, T. J.; Lilley, D. M. J.; Ha, T. *Biophys. J.* **2004**, *87*, 2798−2806.
(48) Lu, H. P.; Xie, X. S. *Nature* **1997**, *385*, 143−146.
(49) Seidel, C. A. M.; Schulz, A.; Sauer, M. H. M. *J. Phys. Chem.* **1996**, *100*, 5541−5553.
(50) Kim, J.; Doose, S.; Neuweiler, H.; Sauer, M. *Nucleic Acids Res.* **2006**, *34*, 2516−2527.
(51) Sauer, M. *Angew. Chem., Int. Ed.* **2003**, *42*, 1790−1793.
(52) Neuweiler, H.; Doose, S.; Sauer, M. *Proc. Natl. Acad. Sci. U.S.A.* **2005**, *102*, 16650−16655.
(53) Holman, M. W.; Liu, R.; Adams, D. M. *J. Am. Chem. Soc.* **2003**, *125*, 12649−12654.
(54) Issac, A.; von Borczyskowski, C.; Cichos, F. *Phys. Rev. B* **2005**, *71*, 161302/1−16130.2/4.
(55) Schuster, J.; Cichos, F.; von Borczyskowski, C. *Appl. Phys. Lett.* **2005**, *87*, 051915/1−05191.5/3.
(56) Yeow, E. K. L.; Melnikov, S. M.; Bell, T. D. M.; De Schryver, F. C.; Hofkens, J. *J. Phys. Chem. A* **2006**, *110*, 1726−1734.
(57) Hoogenboom, J. P.; van Dijk, E. M. H. P.; Hernando, J.; van Hulst, N. F.; Garcia-Parajo, M. F. *Phys. Rev. Lett.* **2005**, *95*, 097401/1−09740.1/4.
(58) Zondervan, R.; Kulzer, F.; Orlinskii, S. B.; Orrit, M. *J. Phys. Chem. A* **2003**, *107*, 6770−6776.
(59) Tinnefeld, P.; Buschmann, V.; Weston, K. D.; Biebricher, A.; Herten, D.-P.; Piestert, O.; Heinlein, T.; Heilemann, M.; Sauer, M. *Rec. Res. Dev. Phys. Chem.* **2004**, *7* (Pt. 1), 95−125.
(60) Tinnefeld, P.; Herten, D. P.; Sauer, M. *J. Phys. Chem. A* **2001**, *105*, 7989−8003.
(61) Ha, T.; Xu, J. *Phys. Rev. Lett.* **2003**, *90*, 223002/1−22300.2/4.
(62) Deniz, A. A.; Dahan, M.; Grunwell, J. R.; Ha, T.; Faulhaber, A. E.; Chemla, D. S.; Weiss, S.; Schultz, P. G. *Proc. Natl. Acad. Sci. U.S.A.* **1999**, *96*, 3670−3675.
(63) Heinlein, T.; Biebricher, A.; Schlueter, P.; Roth, C. M.; Herten, D.-P.; Wolfrum, J.; Heilemann, M.; Mueller, C.; Tinnefeld, P.; Sauer, M. *ChemPhysChem* **2005**, *6*, 949−955.
(64) Tinnefeld, P.; Hofkens, J.; Herten, D.-P.; Masuo, S.; Vosch, T.; Cotlet, M.; Habuchi, S.; Muellen, K.; De Schryver, F. C.; Sauer, M. *Chem. Phys. Chem.* **2004**, *5*, 1786−1790.
(65) Turro, N. J. *Modern molecular photochemistry*, 1st ed.; The Benjamin/Cummings Publishing Co., Inc.: Menlo Park, CA, 1978; p 628.
(66) Ha, T. *Methods* **2001**, *25*, 78−86.
(67) Dittrich, P. S.; Schwille, P. *Appl. Phys. B—Lasers Opt.* **2001**, *73*, 829−837.

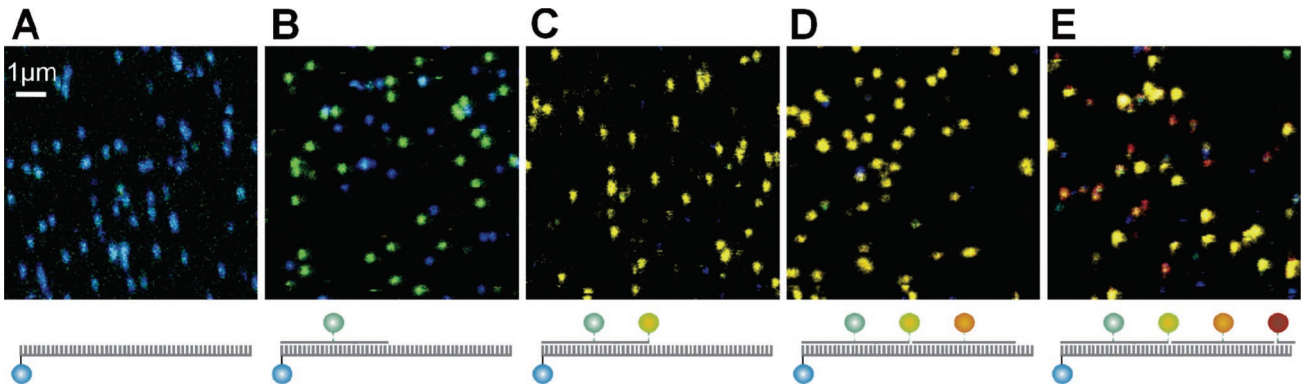

Figure 2. Confocal spectrally resolved fluorescence intensity images of hybridized photonic wires on a cover slide (detection channels 1−4 are encoded in blue, green, yellow, and red). (A) Image of the immobilized single-stranded 60mer carrying biotin on the 3′-end and RhG on the 5′-end. (B) RhG,TMR-labeled dsDNA immobilized after hybridization. In the following images, differently labeled oligonucleotides were subsequently hybridized to the immobilized 60mer template strand. (C) Hybridization of the TMR,ATTO590-labeled 20mer oligonucleotide. (D) Fluorescence images after hybridization of the ATTO647N oligonucleotide to the sample displayed in (C); fluorescence spots show a darker yellow color than in (C). (E) Finally, the Cy5.5 oligonucleotide was hybridized on the same cover slide. A mixture of mainly dark yellow and orange-red spots is evident. (Average excitation intensity at 488 nm, 1 kW/cm^2; 50 nm/pixel; 1 ms/pixel integration time).

wavelength,[59,68−70] thus opening up new photobleaching pathways. As up to five different chromophores are involved in the construction of the DNA-based photonic wires investigated in this work, the selection of chromophores and the elaboration of appropriate conditions to increase their photostability are key parameters to successfully improve the performance of surface-anchored photonic wires.[71]Recently, it has been shown that all chromophores in multichromophore applications should stem from one dye class to ensure similar recipes for optimal performance. Accordingly, carborhodamine and rhodamine derivatives can be merged into one photophysical class, as they show similar dependencies. For these dye classes, the best results with respect to brightness, photostability, and blinking were obtained in PBS, pH 7.4, upon addition of 100 mM MEA.[71] With the advantage of covering a wide spectral range, we decided to use the rhodamine dyes Rhodamine Green (RhG), Tetramethylrhodamine (TMR), ATTO590, and LightCyclerRed (LCR) and the carborhodamine ATTO647N to construct photonic wires. To extend photonic wires beyond the spectral availability of rhodamine dyes and to show the consequences of employing dyes from different classes, we used Cy5.5 as the final emitter.

Immobilization of Photonic Wires. After free rotational mobility of the chromophores on BSA-coated surfaces was confirmed using polarization-modulated excitation spectroscopy,[28,71] the template DNA carrying RhG was immobilized via the biotin tag. Figure 2 demonstrates the subsequent in situ synthesis of DNA-based photonic wires monitored by scanning confocal fluorescence imaging microscopy on four spectrally separated detection channels. Figure 2A shows the RhG-labeled template strand immobilized on a BSA/biotinylated BSA-coated cover slide. As RhG primarily emits on the shortest wavelength channel (Table 1), the false-color image in Figure 2A shows blue spots exclusively (channels 1−4 are false-color encoded in blue, green, yellow, and red). In Figure 2B, the template strand was hybridized to a complementary 20mer carrying TMR only, prior to immobilization to the surface. A fraction of ∼60% of the photonic wires exhibits primarily fluorescence from TMR (green spots), indicating successful hybridization and subsequent efficient FRET. Clearly better results are demonstrated in Figure 2C, where the dual-labeled complementary 20mer was added to the solution *after* immobilization of the 60-bp template strand (i.e., using the in situ hybridization strategy). Here, efficient energy transfer from RhG over TMR to ATTO590 is observed for >95% of all photonic wires.

The same surface was further incubated with the ATTO647N oligonucleotide, yielding a high fraction of spots exhibiting primarily fluorescence from ATTO647N, as indicated by darker yellow spots (Figure 2D). Both ATTO590 and ATTO647N mainly emit on the third (yellow) detector (see Table 1), but the higher contribution of ATTO647N emission on the fourth (red) detector leads to a darker yellow in the false-color image. Finally the third complementary oligonucleotide, carrying Cy5.5, was hybridized to the template DNA (Figure 2E). Cy5.5-dominated emission should yield red spots, but many molecules seen in Figure 2E are dominated by ATTO647N emission. Obviously, the last hybridization step is less efficient. Furthermore, spots carrying Cy5.5 show lower fluorescence intensities and are comparatively dim (see orange/red spots in Figure 2E). The lower fluorescence quantum yield of Cy5.5, $\Phi_{fl} = 0.28$ compared to $\Phi_{fl} = 0.65$ for ATTO647N, can partly account for the lower brightness of these five-chromophore wires. In addition, the combination of low quantum yield and inefficient individual energy-transfer steps (i.e., each energy-transfer step occurs with an efficiency <100%) yields spots that do not appear purely red, as expected from the dye emission patterns given in Table 1. However, inspection of the false-color images shown in Figure 2 clearly demonstrates that the applied immobilization strategy homogenizes energy-transfer efficiencies in DNA-based photonic wires. Compared to previous reports, the spectral heterogeneity between the spots (static heterogeneity) and within the spots (dynamic heterogeneity) is strikingly reduced.[3,22,72]

(68) Ying, L. M.; Xie, X. S. *J. Phys. Chem. B* **1998**, *102*, 10399−10409.
(69) Tinnefeld, P.; Weston, K. D.; Vosch, T.; Cotlet, M.; Weil, T.; Hofkens, J.; Mullen, K.; De Schryver, F. C.; Sauer, M. *J. Am. Chem. Soc.* **2002**, *124*, 14310−14311.
(70) Eggeling, C.; Widengren, J.; Brand, L.; Schaffer, J.; Felekyan, S.; Seidel, C. A. M. *J. Phys. Chem. A* **2006**, *110*, 2979−2995.
(71) Heilemann, M.; Kasper, R.; Tinnefeld, P.; Sauer, M. manuscript in preparation.
(72) Sanchez Mosteiro, G.; van Dijk, E. M. H. P.; Hernando, J.; Heilemann, M.; Tinnefeld, P.; Sauer, M.; Koberling, F.; Patting, M.; Wahl, M.; Erdmann, R.; van Hulst Niek, F.; Garcia Parajo, M. F. *J. Phys. Chem. B*, published online Dec 5, 2006 http://dx.doi.org/10.1021/jp064701f.

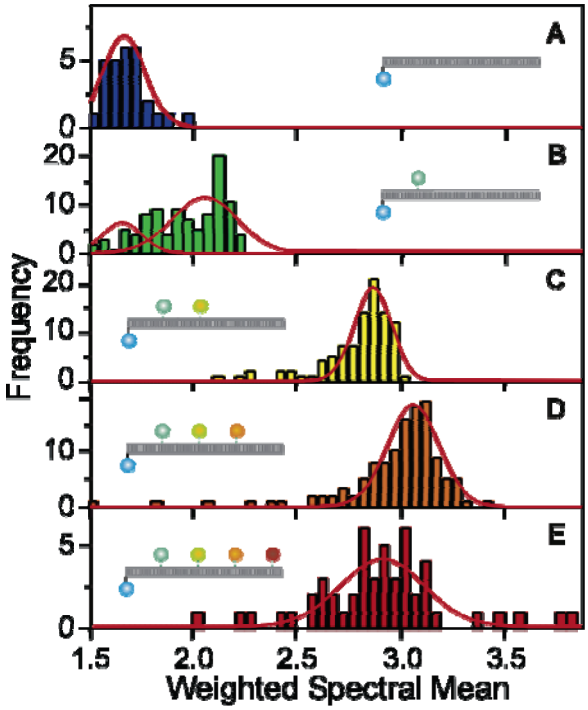

Figure 3. Histograms and Gaussian fits of background-corrected weighted spectral means (WSM values) determined from images as presented in Figure 2. Additionally, the photonic wires are schematically presented.

To further analyze the energy-transport properties of photonic wires immobilized in solution, spot-integrated statistics using a spot-finding algorithm were determined. For a quantitative analysis of the spectral characteristics, we define the weighted spectral mean (WSM) parameter (eq 2), where j is the number

$$\mathrm{WSM} = \frac{\sum_j j\, I_{\mathrm{det}\,j}}{\sum_j I_{\mathrm{det}\,j}} \qquad (2)$$

of the detector (with $j = 1, 2, 3, 4$ for detectors blue, green, yellow, and red) and $I_{\mathrm{det}\,j}$ is the number of photon counts per spot, respectively. The WSM parameter therefore presents a projection of the multidimensional spectral properties into one number and allows a first straightforward characterization of the emission and heterogeneity of photonic wires. A hypothetical molecule exclusively emitting on the first (blue) detector yields a WSM = 1, whereas a purely red-emitting molecule yields a WSM = 4. Applied to the chromophores used in our experiments, donor-only emission from RhG should yield a WSM value of 1.53, whereas exclusive emission from the fifth dye (Cy5.5) is expected to yield a WSM of 3.99 (compare values in Table 1).

Figure 3 shows the WSM distributions of photonic wires discussed in Figure 2. Narrow distributions allow unambiguous assignment of every spot to a photonic wire with a defined composition of chromophores. The population of RhG emission (Figure 3A), for example, peaks at WSM = 1.7, i.e., slightly higher than expected from the ensemble spectrum (Table 1). The population of TMR-hybridized wires is broader, as expected from the image in Figure 2B, and a WSM of 2.1 is determined for the population of TMR-dominated emission. The histogram in Figure 3B nicely reflects the greater heterogeneity, as the DNA was not hybridized on the surface but in solution before immobilization. In contrast, photonic wires built on the solid support directly exhibit a single distribution, as for the combined TMR−ATTO590 oligonucleotide, with a mean WSM of ~ 2.8. Since ATTO590 and ATTO647N have similar emission patterns with respect to the filter set used (Table 1), the success of the hybridization of the ATTO647N oligonucleotides is indicated only by the slightly darker yellow color of spots in Figure 2D compared to Figure 2C. WSM-value histograms now help to quantify this hybridization step. The shift of the distribution in Figure 3D compared to Figure 3C from WSM = 2.8 to WSM = 3.1 points toward almost quantitative hybridization. Unexpectedly, this trend toward higher WSM values does not continue for hybridization of the third oligonucleotide, carrying the fifth chromophore, Cy5.5 (see Figures 2E and 3E). Instead, the photonic wire containing five chromophores exhibits a mean WSM value of only 2.9.

The narrow widths of the WSM distributions indicate that FRET occurs with high efficiency at least up to the fourth chromophore, whereas the histogram in Figure 3E indicates imperfect energy transfer in the five-chromophore photonic wire. Taking into account the different quantum yields and their spectral separation on the detector channels (see Table 1), together with the theoretically expected energy-transfer efficiency of ~0.97 (calculated on the basis of spectral overlap and an inter-chromophore distance of 10 bp while assuming free rotation of the chromophores) between two chromophores, a perfectly working photonic wire should exhibit a WSM value of 3.02 over five chromophores and 2.95 over four chromophores.

Since the WSM parameter constitutes only a one-dimensional projection of the emission pattern, it does not comprise the full information included in the detection on four spectrally separated channels. To further distinguish between the emissions of ATTO647N and Cy5.5, an additional parameter which reflects the relative emission of the third (yellow) versus the fourth (red) channel is necessary. Scatter plots depicting the fractional intensity on the fourth channel with respect to the sum intensity on channels three and four (fractional intensity $F_{3,4} = I_{\mathrm{det}\,4}/(I_{\mathrm{det}\,3} + I_{\mathrm{det}\,4})$) versus the WSM value of the wires were calculated (Figure 4). The four-chromophore wire carrying ATTO647N as the final acceptor shows a distribution around a fractional intensity $F_{3,4}$ of 0.28 and a WSM value of 3.1 (Figure 4A). On the other hand, Figure 4B shows a similar graph obtained for the five-chromophore wire, which clearly reveals the existence of two populations. We ascribe the additional population in Figure 4B, with a fractional intensity $F_{3,4}$ of 0.53 and a WSM value of 2.8, to photonic wires emitting primarily from Cy5.5 In Figure 4B, the population of the five-chromophore wire comprises ~45% of all molecules. Accordingly, the two-dimensional representation is able to clearly resolve the subpopulation of photonic wires operating over the full range of five chromophores.

Several reasons can account for the reduced fraction of intact five-chromophore wires. First, it is known that certain cyanine derivatives, such as Cy5 or Cy5.5, frequently show inactive subpopulations, which do not act as FRET acceptors.[62,63,73] Second, the measurement conditions (addition of MEA but no

(73) Ha, T. J.; Ting, A. Y.; Liang, J.; Deniz, A. A.; Chemla, D. S.; Schultz, P. G.; Weiss, S. *Chem. Phys.* **1999**, *247*, 107−118.

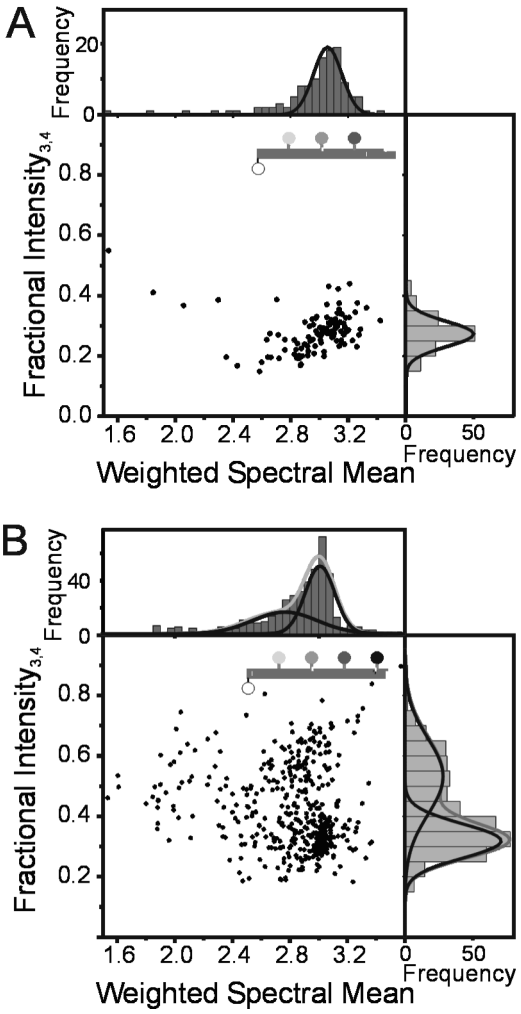

Figure 4. Scatter plots of the fractional intensity $F_{3,4} = I_{\text{det }4}/(I_{\text{det }3} + I_{\text{det }4})$ versus WSM for the four-chromophore (lacking Cy5.5) (A) and five-chromophore (B) photonic wires and corresponding Gaussian fits. The two-dimensional representation allows resolving different subpopulations present in the case of the five-chromophore photonic wire.

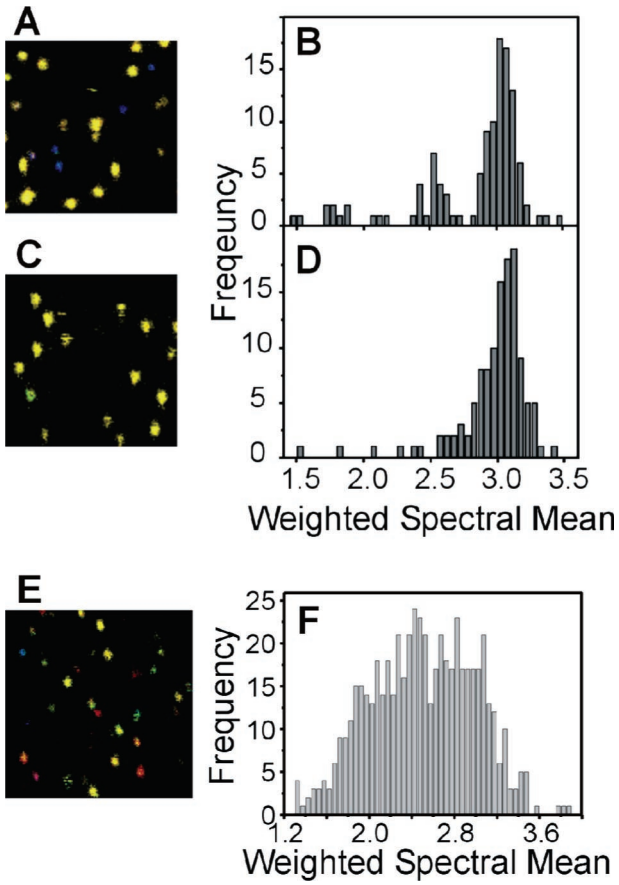

Figure 5. Dissecting the sources of heterogeneity. (A) False-color image of the four-chromophore photonic wire immobilized after hybridization in solution and the corresponding WSM histogram (B). (C,D) For comparison, the corresponding image and WSM histogram obtained for the same wire hybridized on the surface (using the in situ hybridization strategy). (E) False-color image of the corresponding five-chromophore photonic wires immobilized on dry glass cover slides. A broad distribution of WSM values is obtained (F), mainly due to the fixation of transition dipoles and increased inhomogenous broadening.

removal of oxygen) were optimized for rhodamine dyes so that the photochemical stability of Cy5.5 is substantially lower.[71] This results in early photobleaching and subsequent decrease of energy-transfer efficiency to the final acceptor.[74] Third, the overall lower brightness of wires carrying Cy5.5 decreases the fraction of wires detected by the automated spot recognition procedure. Finally, the hybridization efficiency of the last complementary oligonucleotide might be hindered sterically because that oligonucleotide is located closest to the protein surface.

In the following, we dissect some of the factors that were crucial to obtain the demonstrated homogeneity with a very high fraction (>90%) of intact systems up to the fourth chromophore and of about 45% up to the fifth chromophore. Figure 5 compares the performance of the four-chromophore wire hybridized in solution prior to immobilization to that of the same wire hybridized in situ on the cover slide.

The subpopulations appearing below WSM values of 2.8 in Figure 5B represent imperfectly hybridized wires and are more frequently observed when wires had been prepared in solution prior to immobilization. Surprisingly, the main imperfect wire population occurs at a WSM of ~2.6, i.e., at a WSM value which does not represent a defined sample composition (compare Figure 3 and Table 1). This population also appears in Figure 3C and is responsible for the slight asymmetry of the peak at a WSM value of 2.8. Evidently, pre-hybridization of wires in solution yields a lower fraction of intact photonic wires. The in situ hybridization strategy on the slide increases the yield of intact wires by ~22%.

A drastically different picture emerges when photonic wires are directly adsorbed on bare glass cover slides, as shown in the false-color image of a corresponding five-chromophore photonic wire in Figure 5E.[3,22,72] The WSM histogram obtained under dry conditions is significantly broader than that for wires immobilized in solution, and no individual subpopulations can be resolved. We therefore conclude that the freezing-out of conformations, distance variations, and orientations on the dry glass surface are the main sources of heterogeneity observed from rigidly immobilized photonic wires. That is, the flexibility of photonic wires anchored in solution is the key to increased homogeneity.

Fluorescence Intensity Transients of Individual Photonic Wires. Detailed information about the energy-transfer paths can

(74) Morgan, M. A.; Okamoto, K.; Kahn, J. D.; English, D. S. *Biophys. J.* **2005**, *89*, 2588−2596.

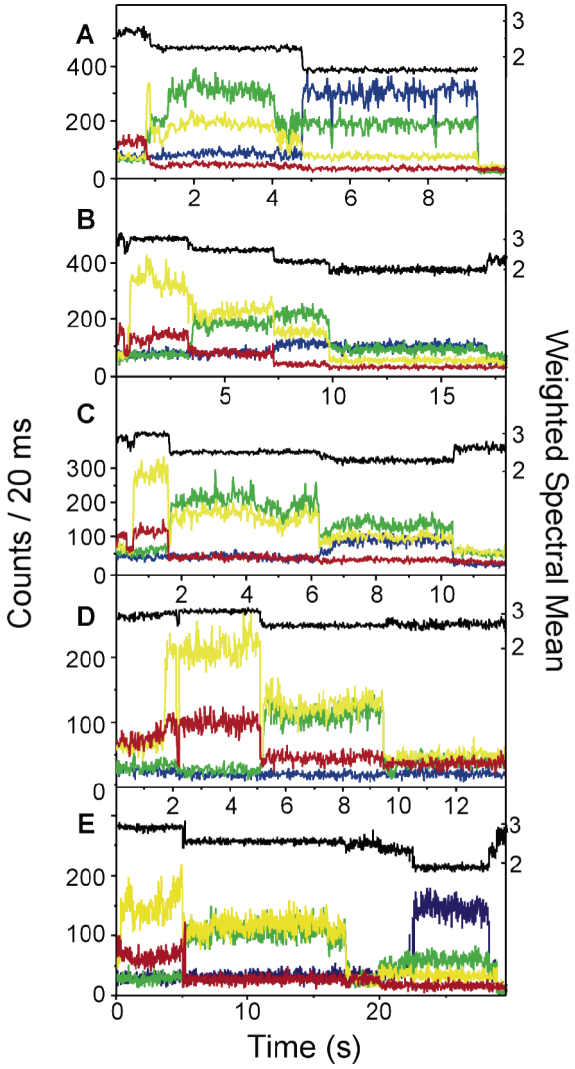

Figure 6. (A−E) Representative fluorescence transients of five-chromophore photonic wires. The intensity on the spectrally separated detection channels is shown in blue, green, yellow, and red, respectively. The transients of the WSM values are shown for better visualization of the subsequent blue-shifted emission (black).

be obtained from fluorescence transients of single photonic wires. Figure 6 shows example transients exhibiting distinct sections of comparably stable emission with a defined intensity distribution between the four channels. The sections are separated by sudden changes of the spectral characteristics of fluorescence emission due to bleaching events of individual chromophores within the wire. At their beginning, all transients exhibit emission on the red channel with WSM values around ∼2.9, representing intact photonic wires. After less than 1 s, photobleaching of Cy5.5 generally occurs, associated with an increase in overall intensity and a change in the emission pattern. The increase in fluorescence intensity as a result of Cy5.5 photobleaching confirms the idea that five-chromophore photonic wires are less bright due to the lower quantum efficiency of the final acceptor Cy5.5, resulting in lower WSM values. Subsequently, stepwise photodestruction accompanied by a blue-shifted emission is observed, confirming that the energy is transferred stepwise through the photonic wires. The order of successive photobleaching from red to blue is expected, as the probability of photobleaching is proportional to the time a chromophore spends in its excited state.

However, in contrast to expectation, photobleaching does not always occur in the intended order, and five photobleaching steps cannot always be resolved. In Figure 6A, a section representing primarily emission from ATTO647N is missing, indicating that photobleaching of Cy5.5 and that of ATTO647N coincide. On the other hand, Figure 6B portrays a photonic wire that exhibits all five expected intensity levels and successive bleaching of chromophores. Interestingly, a collective off-state at the end of the Cy5.5-dominated section of the transient is observed (see also Figure 6C).[61,75,76] Up to about 3 s, the transient in Figure 6B is dominated by ATTO647N, indicated by the high fluorescence intensity on the yellow channel as well as on the red channel. From 3 to 7 s, the fluorescence is dominated by ATTO590, exhibiting dominant emission on the yellow channel and a substantial fraction on the green channel. This part is followed by TMR-dominated emission from 7 to 10 s. However, it cannot simply be explained why the overall intensity decreases in the course of the transient, which is in particular associated with the apparent photobleaching step of TMR after ∼10 s. It is likely that TMR does not completely photobleach after 10 s but enters a weakly emitting state. This is also corroborated by the fact that, after photobleaching of RhG, the fluorescence intensity on the green and yellow channels is still significantly above the background count rate, implying direct excitation of the remaining TMR species (direct excitation of TMR at 488 nm is about 8%, while direct excitation of the other chromophores is negligible). Similar observations are made in the transients shown in Figure 6D,E.

Interestingly, fluorescence transients of photonic wires reveal more subtle interactions and heterogeneities. For example, the transient shown in Figure 6A exhibits fluorescence on the blue channel throughout the observation time of the photonic wire. From the background-subtracted emission on the blue channel, it can be deduced that the energy-transfer efficiency from RhG to the other chromophores is substantially lower than expected, i.e., only about 83% instead of 97%. In the first section of the transient, the blue channel shows slightly higher fluorescence intensity than the green channel. As 37% of the RhG emission is detected on the green channel, contributions from the other dyes, i.e., TMR and ATTO590, must be very small, indicating almost quantitative energy transfer from TMR via ATTO590 to ATTO647N. Similar emission patterns with lower energy-transfer efficiencies for the first step compared to the subsequent energy-transfer steps are observed frequently (see also Figure 6B,E). In some cases, a fraction of the relatively low energy-transfer yield between RhG and TMR is compensated by non-nearest-neighbor energy transfer, i.e., direct FRET between RhG and ATTO590. In the transient of Figure 6B, for example, emission of RhG is partly restored when ATTO590 is photobleached after ∼7 s.

Sections with a WSM value of ∼2.6 are also observed in some transients of single photonic wires (compare Figure 5 with Figure 6D between 5 and 10 s or with Figure 6E between 5 and 17 s), which might represent a low-FRET efficiency state between TMR and ATTO590. However, the spectral data alone are insufficient to characterize this observation.

(75) Hofkens, J.; Maus, M.; Gensch, T.; Vosch, T.; Cotlet, M.; Kohn, F.; Herrmann, A.; Mullen, K.; De Schryver, F. *J. Am. Chem. Soc.* **2000**, *122*, 9278−9288.
(76) Tinnefeld, P.; Buschmann, V.; Weston, K. D.; Sauer, M. *J. Phys. Chem. A* **2003**, *107*, 323−327.

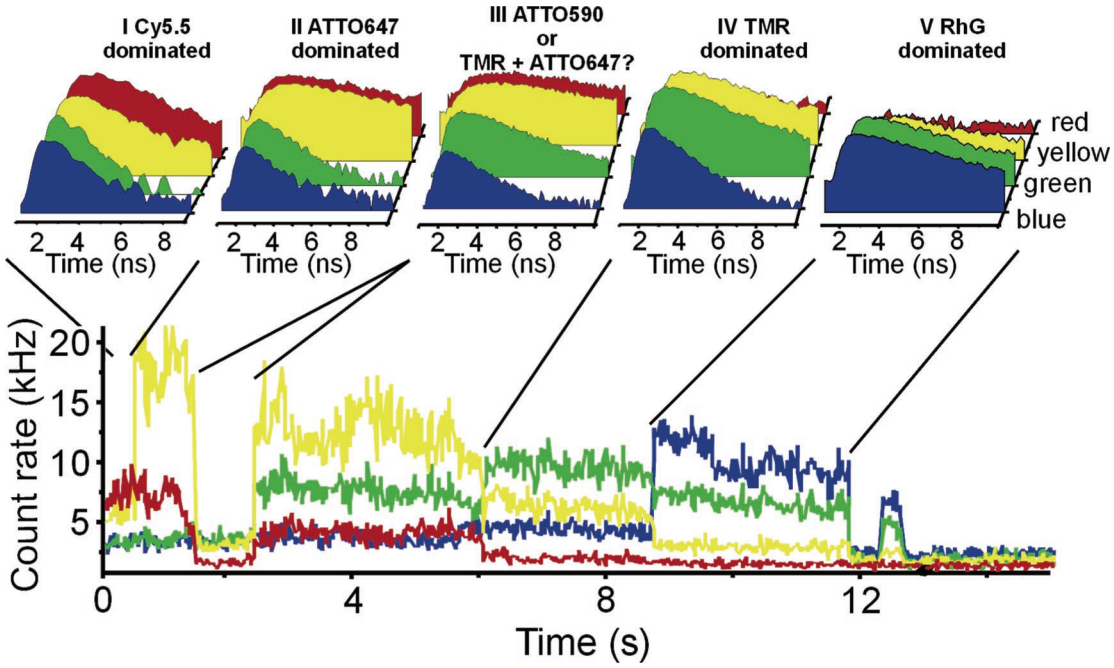

Figure 7. Spectrally resolved and time-resolved intensity transient of a single five-chromophore photonic wire in PBS (excitation power, 20 μW; binning, 20 ms). Fluorescence decays for each section and of all four detector channels are shown in the upper panels. In addition, a collective off-state is visible around 2 s. The subsequent hypsochromic shift of the emission indicates stepwise photodegradation of the device.

Fluorescence Lifetime Measurements. As explained in the previous section, a precise dissection of each individual transfer step is not always possible with the spectral information only. The additional fluorescence lifetime information can lift the ambiguity resulting from the investigation of a five-chromophore FRET system with four spectrally separated detection channels, involving significant spectral crosstalk between the channels. As an additional and independent parameter, fluorescence lifetime gives access to a more detailed description of energy transfer, including leaks and traps as well as unfavorable relative orientations and photobleaching orders.

An exemplary transient of a five-chromophore wire is shown in Figure 7. The transient can be divided into five sections, I−V, characterized by their spectral distributions. In addition, fluorescence decays for each section are shown. From a first inspection, one is tempted to assign the different intensity distributions to successive photobleaching events of the wire, starting from Cy5.5 to RhG. The fluorescence decays show strongly quenched emission on the shorter wavelength channels (blue and green) for sections I−III, whereas both the red and the yellow channels are dominated by emission from the final emitter. Quenching on the short-wavelength channels directly reflects stepwise energy transfer to the lower energy chromophores. Section IV is obviously dominated by TMR emission with corresponding quenched emission on the blue channel. Section V represents emission solely from RhG, supported by identical decays on the first three channels.

A closer inspection of the decays reveals more information. For example, a dequenching in several steps is observed on the green channel: while strongly quenched in the first two sections, it is partially dequenched in the third section and completely dequenched in the fourth section, which is the section of TMR-dominated emission. Two scenarios may explain this observation for the green channel in section III: (i) ATTO647N photobleached, and TMR and ATTO590 exhibit unfavorable transition dipole orientations, implying that in section II much of the TMR quenching was induced by direct energy transfer to ATTO647N, or alternatively, (ii) ATTO590 photobleached after about 2.5 s and the emission pattern, which appears typical for ATTO590, represents in fact the sum of partly quenched TMR emission and intermediate energy transfer to ATTO647N.

Subsequent photobleaching allows us to analyze the transient in reverse chronological order, i.e., starting at the end of a transient, where the system is simple, and then proceeding toward sections exhibiting more complexity, under the assumption that the parameters obtained for the posterior sections of the transient are still valid in the earlier sections (i.e., excluding dynamic heterogeneity). The last section of the transient is dominated by RhG emission. Section IV is then assumed to represent emission from TMR with unknown intensity distribution on the different detection channels and RhG being quenched by energy transfer to TMR. As TMR does not emit on the blue channel, the remaining intensity on the blue channel is ascribed to emission from RhG. A set of linear equations then allows the determination of RhG contribution to the overall emission as well as its distribution between the channels. As a result, the energy-transfer efficiency is determined as $E_{1,2} = 0.73$.

To analyze section III, the two possibilities that either (i) ATTO647 or (ii) ATTO590 photobleached after ~2.5 s have to be considered. Assuming constant emission characteristics for RhG and TMR and using the known spectral characteristics of ATTO590, one obtains a system of six linear equations with six variables for case (i), i.e., ATTO647N bleached. The variables are the contributions of the three chromophores and the distribution of ATTO590 emission on channels 2−4. Accordingly, emission in that part of the transient stems from RhG to ~13%, from TMR to ~10%, and from ATTO590 to ~76%. Including quantum efficiencies,[3] an overall transfer efficiency of $E = 0.86$ is calculated. The calculation further yields a distribution of ATTO590 on the four channels of 0.0/

Table 2. Fitted Fluorescence Decay Times of the Photonic Wire in Figure 7[a]

	blue	green	yellow		red	
	τ (ns)/χ^2	τ (ns)/χ^2	τ_1 (ns)/χ^2/a_1	τ_2 (ns)/a_2	τ_1 (ns)/χ^2/a_1	τ_2 (ns)/a_2
V	3.4/1.01	3.31/0.99				
IV	0.78/1.74	2.95/1.15	3.19/2.0			
III	0.69/2.0	1.73/1.35	4.0/1.13/1.28	0.86/−0.28	3.6/1.11/1.95	1.7/−0.95
II	0.25/1.21	0.66/1.35	3.5/1.96/1.24	0.65/−0.24	3.7/1.37/1.12	0.41/−0.12
I	0.23/1.1	0.47/1.08	0.95/1.36		1.6/1.51/1.32	0.32/−0.32

[a] The quality of the decay fits was assessed by means of the reduced chi-squared statistical parameter (χ^2). Decays could be satisfactorily described by one- or two-exponential fits ($I(t) = \sum a_i \exp(-t\,\tau_i^{-1})$).

0.23/0.61/0.16, in reasonable agreement with the ensemble values presented in Table 1.

Assuming that ATTO590 bleached after 2.5 s (case (ii)), an analogous calculation yields a RhG contribution to the overall intensity of 13%, a TMR contribution of 42%, and an ATTO647N contribution of 45%, with a reasonable spectral distribution of 0.0/0.0/0.74/0.26 for ATTO647N. Accounting for the different fluorescence quantum yields, an overall transfer efficiency of $E = 0.53$ is obtained, which is in neat accordance with expected values, including a highly efficient energy-transfer step and an intermediate efficient transfer step, recalling the distance between TMR and ATTO647N of 20 bp and a Förster radius $R_0 = 57$ Å for the FRET pair TMR−ATTO647N.[30,31] Due to the fact that the two possibilities (i) and (ii) yield reasonable results with respect to energy transfer and dye contributions, intensity ratio measurements alone cannot distinguish between the two possibilities. However, fluorescence lifetime experiments enable us to resolve this ambiguity. In case (i), the fluorescence decay of the green channel would constitute the sum of a strongly quenched TMR plus a fraction of the strong ATTO590 emission, with a long fluorescence lifetime component of ∼3.6 ns (fitted decay times for the different sections of the wire shown in Figure 7 are summarized in Table 2). The relative amplitudes of the contributions would then be ∼12% for TMR and ∼88% for ATTO590. In contrast, the green channel exhibits a monoexponential decay and does not include similar long lifetime components as the yellow and red channels. Therefore, we conclude that ATTO590 bleached and case (ii) is observed. From the reduced lifetime of TMR, a FRET efficiency E of 44% ($E = 1 - \tau_D'/\tau_D$, where τ_D' and τ_D are the donor fluorescence decay times in the presence and absence of an acceptor, respectively) is calculated, in reasonable agreement with the value determined from the relative intensities.

Section II shows data of an intact four-chromophore wire up to ATTO647N with a fluorescence decay time of ∼3.6 ns. Here, the relative contributions of the dyes cannot easily be calculated because there are seven unknown variables and only six linear equations. Inspection of some aspects of the transient and the fluorescence lifetime, however, indicates that energy transfer from ATTO590 is very efficient. This is because the intensity on the green channel does not change upon ATTO590 bleaching after 1.5 s. As ATTO590 emits to 33% on the green channel (see Table 1), a change is expected in the case of measurable ATTO590 emission. Furthermore, the same emission distribution on the four channels for ATTO647N in sections II and III can be maintained only if ATTO590 is not contributing to the emission in section II. Hence, the overall energy-transfer efficiency in section II of the transient can be estimated as $E =$ 85%. As the background-corrected WSM value of ∼3.0 for section II is also typical for wires carrying ATTO647N as the final acceptor (see Figure 3D), we conclude that the homogeneous distribution around a WSM value of ∼3.1 is similar to an average overall transfer efficiency of ∼85−88% over a distance of ∼10 nm.

In section I, the total fluorescence intensity is significantly reduced owing to the lower fluorescence quantum yield of Cy5.5. As Cy5.5 exclusively emits on the red channel, a significant emission from ATTO647N is evident on the yellow channel, suggesting that this last energy-transfer step is less efficient. Assuming only very low emission from ATTO590, the relative contribution of the dyes and the energy-transfer efficiency can be calculated. For the final step from ATTO647N to Cy5.5, an energy-transfer efficiency of $E_{4,5} = 0.74$ and an overall energy-transfer efficiency of $E = 0.68$ are obtained. The background-corrected WSM value of section I of the transient is 3.16; i.e., this particular photonic wire belongs to the more effective wires (see the distribution of WSM values in Figures 4E and 5B for comparison). On average, we estimate that the overall energy-transfer efficiency over five chromophores, using Cy5.5 as the final acceptor, is $E \approx 0.63$, i.e., significantly lower than initially expected and also strikingly lower than the maximum values obtained on a glass surface in the range of $E \approx 0.90$.[3,22]

Our detailed analysis demonstrates that, in particular, the first and the last energy-transfer steps are less efficient than expected from theoretical considerations. These are likely caused by unfavorable relative orientations due to interactions with the environment, thus yielding reduced κ^2 values. In addition, as chromophore−DNA interactions can likely prevail much longer than expected, they can have a profound influence on distance determinations based on FRET.[39] Furthermore, it was shown that, for highly efficient energy transfer, κ^2 can deviate considerably from 2/3.[77]

As expected for energy transfer, rise times are observed in the fluorescence decays in the first three sections of the transient shown in Figure 7 (see also Table 2). For the decays recorded in the last two sections, additional components do not improve the fit, and rise times are not resolved due to low photon statistics and crosstalk of short components from the donor dye into the acceptor channel. It is interesting to note that, in sections I and II, RhG exhibits a shorter fluorescence lifetime than in later sections, giving further evidence for additional quenching interactions between non-nearest-neighboring dyes. That is, upon bleaching of remote dyes, the fluorescence lifetime of RhG is already partly dequenched. The fact that a large fraction of the dequenching has already occurred in section III provides additional evidence that ATTO590 bleached after 2.5 s and

(77) Schuler, B.; Lipman, E. A.; Steinbach, P. J.; Kumke, M.; Eaton, W. A. *Proc. Natl. Acad. Sci. U.S.A.* **2005**, *102*, 2754−2759.

explains why the overall energy-transfer efficiency can be higher than for the individual energy-transfer step between RhG and TMR in section II.

The long off-state between sections II and III is likely a nonfluorescent but still absorbing photobleaching intermediate of ATTO590. Interestingly, neither the intensity of the first two channels nor the decays in these channels change, indicating that the photobleaching intermediate has absorption properties similar to those of the original ATTO590 but does not promote further energy transfer to ATTO647N. The fact that the first two channels show identical emission properties can also indicate that, during the off-state, ATTO590 is still in its original ground state but as soon as it becomes excited the fluorescence is quenched by an impurity in the immediate environment, which finally leads to bleaching.

Conclusions

The study of multichromophoric systems is fascinating both from a fundamental scientific view and from the perspective of their applicability as efficient molecular light-guiding devices. As revealed in recent studies, the heterogeneous photophysical properties in multichromophoric systems such as conjugated polymers, multichromophoric dendrimers, or molecular photonic wires remain a challenging problem. In this article, we exploit for the first time the information obtained from multiparameter SMFS measurements to work out solutions to control heterogeneity in complex supramolecular systems. Our approach to the construction of photonic wires by attaching chromophores along a DNA backbone takes advantage of the in situ synthesis (and subsequent hybridization) of wire components under aqueous conditions without perturbation by the surface. Since the approach does not enable precise control of the orientation of the chromophores, homogeneity is achieved by leaving the required conformational freedom for the chromophores to rapidly equilibrate between conformational subpopulations. Selecting suited chromophores, photonic wires with up to four chromophores exhibiting homogeneous emission properties were obtained by a combination of rhodamine and carborhodamine derivatives. Further extension to five chromophores and thus to the far red of the spectrum was achieved by attaching a carbocyanine derivative, Cy5.5. Molecular photonic wires exhibiting ∼85% FRET efficiency over four chromophores could be prepared with >90% yield. Extension to the fifth chromophore yields photonic wires exhibiting overall FRET efficiencies of ∼68% over ∼13.3 nm, with a yield of 45%. The success in obtaining homogeneous energy-transfer efficiencies in DNA-based photonic wires and the characterization of the remaining heterogeneity demonstrate that single-molecule techniques are becoming invaluable for the development of bottom-up molecular devices.

Acknowledgment. The authors thank G. Sanchez Mosteiro, M. F. Garcia-Parajo, and N. F. van Hulst for fruitful collaboration. The authors are grateful for financial support from the Volkswagenstiftung (Grant I/87 094) and the German Academic Exchange Service (DAAD, M.H.).

JA065585X